

X-ray Observation of Mars with Suzaku at Solar Minimum

Kumi ISHIKAWA, Yuichiro EZOE, Takaya OHASHI,

*Department of Physics, Tokyo Metropolitan University, 1-1 Minami-Osawa,
Hachioji, Tokyo, 192-0397*

kumi@phys.se.tmu.ac.jp, ezoe@tmu.ac.jp, ohashi@tmu.ac.jp

Naoki TERADA,

*Department of Geophysics, Tohoku University, 6-3 Aoba, Aramaki-za, Aoba, Sendai, Miyagi,
980-8578*

teradan@stpp.gp.tohoku.ac.jp

and

Yoshifumi FUTAANA

*Swedish Institute of Space Physics, Box 812, SE-98128 Kiruna, Sweden
futaana@irf.se*

(Received 2011 May 20; accepted 2011 August 29)

Abstract

Mars was observed in X-rays during April 3–5 2008 for 82 ksec with the Japanese Suzaku observatory. Mars has been known to emit X-rays via the scattering of solar X-rays and via the charge exchange between neutral atoms in the exosphere and solar wind ions. Past theoretical studies suggest that the exospheric neutral density may vary by a factor of up to 10 over the solar cycle. To investigate a potential change of the exospheric charge exchange emission, Mars was observed with Suzaku at solar minimum. Significant signals were not detected at the position of Mars in the energy band of 0.2–5 keV. A 2σ upper limit of the O VII line flux in 0.5–0.65 keV was 4.3×10^{-5} ph cm $^{-2}$ s $^{-1}$. Comparing this upper limit to the past Chandra and XMM-Newton observations conducted near solar maximum, it was found that the exospheric density at solar minimum does not exceed that near solar maximum by more than 6~70 times.

Key words: planets and satellites: individual (Mars) — X-rays: individual (Mars)

1. Introduction

Martian X-ray emission was discovered in 2001 July with the ACIS-I X-ray CCD detector onboard the Chandra observatory (Dennerl 2002). Thanks to the superb X-ray angular resolution of 0.5 arcsec, the X-ray emission was resolved into two components. The first one is seen at the position of the Martian atmosphere. The observed X-ray spectrum was dominated by a single narrow emission line, which was identified as the 0.53 keV oxygen K_{α} fluorescence line; the total X-ray luminosity due to fluorescence was ~ 4 MW. These spatial and spectral characteristics strongly suggest scattering of solar X-rays in the upper Martian atmosphere, mainly by fluorescence. This type of X-ray emission has been observed in many other planets like Venus, Earth, Jupiter and Saturn (Dennerl et al. 2002; Grader et al. 1968; Gladstone et al. 2002; Ness et al. 2004).

The second component was seen as a faint X-ray halo around Mars that could be traced out to three Mars radii. Within the very limited statistical quality, the overall shape of its X-ray spectrum could be characterized by thermal bremsstrahlung emission with a temperature of 0.2 keV. From the analogy with the X-ray emission from comets (Dennerl et al. 1997; Wegmann et al. 1998), charge exchange emission between high energy solar wind ions and exospheric neutrals was suggested.

The subsequent observation of Mars was conducted on 2003 November 19–21 with XMM-Newton (Dennerl et al. 2006). From the high energy resolution spectroscopy with the Reflection Grating Spectrometer, the presence of ~ 12 emission lines was revealed in the Martian halo. The emission lines were considered to be due to de-excitation of highly ionized C, N, O, and Ne atoms. The He-like O VII triplet was found to be dominated by the spin-forbidden magnetic dipole transition ($2^3S_1 \rightarrow 1^1S_0$). Since the forbidden line is weak compared to the resonance line in astrophysical plasmas (Krasnopolsky et al. 2004), this is a supporting evidence that the Martian halo X-ray emission originates from the charge exchange reaction.

Theoretically, an X-ray flux of the exospheric solar wind X-ray emission is proportional to the incident solar wind flux and the neutral column density of the collisionally thin regions in the exosphere, that is mainly composed of hydrogen, in the line of sight (Cravens 1997). Therefore, the X-ray observation of the Martian halo emission can be a probe to investigate the spatial distribution of hydrogen atoms in the exosphere (Holmström and Barabash 2001) and must be useful to study the exosphere and also an atmospheric escape from Mars. A series of exospheric density models based on measurements with Mariner 6, 7, 9, Viking 1, EUVE, Phobos 2, and Mars Express have been constructed (Anderson 1974; Krasnopolsky & Gladstone 1996; Galli et al. 2006; Chaufray et al. 2008). Some models (Krasnopolsky & Gladstone 1996; Krasnopolsky 2002) of the exospheric density and temperature based on the measurements by Mariner 6, 7 and Viking 1 imply a high dependence on the solar cycle. They suggested that hydrogen exospheric density at solar minimum can be higher than solar maximum due to weaker heating

by solar ultra-violet lights and X-rays. On the other hand, there are some opposite results measured by Mars Express at low solar activity. They indicated no trends to higher exospheric density for low solar activity, comparing to the Mariner 6 and 7 data at solar maximum (Galli et al. 2006; Chaufray et al. 2008). Then, the density of the spatially extended thin atmosphere is not well understood because of the observational difficulty of the exosphere. As a result, a possible variation depending on the solar cycle is unclear.

From this point of view, in this paper, we observed Mars in X-rays for the first time at solar minimum using the Japanese Suzaku observatory. This data set provides us with a good opportunity to compare the Martian halo emission at solar minimum with those observed with Chandra and XMM-Newton near solar maximum.

2. Observation

Suzaku (Mitsuda et al. 2007) observed Mars from 2008 April 3, 08:11 to April 5, 13:00 UT with the X-ray Imaging Spectrometer (XIS; Koyama et al. 2007). The XIS consists of three front-illuminated (FI) CCDs (XIS0, 2, 3) and one back-illuminated (BI) CCD (XIS1). These CCDs cover the energy range of 0.2–12 keV. Due to the low-Earth orbit of Suzaku and large effective area, the XIS has one of the lowest particle backgrounds among all X-ray CCDs in currently available X-ray observatories. Therefore, Suzaku is favorable for the spatially extended emission of Mars, i.e., the Martian halo emission. In this paper, we used the XIS 0, 1, and 3 data. The XIS2 data was unusable at the time of this observation due to, most probably, micro-meteoroid impacts.¹

During the Suzaku observation, heliocentric and geocentric distances of Mars were 1.7 and 1.4 AU, respectively. The average phase angle (Sun-Mars-Earth) and the elongation angle (Sun-Earth-Mars) was 37.0 degree and 87.2 degree, respectively. Mars had an apparent diameter of 6.8 arcsec and a visual magnitude of m_V was 0.86. An optical loading to the XIS was thought to be negligible in this observations, because no optical loading effect was seen when Suzaku observed an optically brighter object, i.e., Jupiter (Ezoe et al. 2010). Although the visual surface brightness of Mars was brighter than Jupiter during the past Suzaku observation (Jupiter and Mars were 5.5 and 4.7 mag per square arcsec during each Suzaku observation, respectively), the effective surface brightness of Mars when observed with Suzaku should be lower because the apparent optical size of Jupiter is larger than that of Mars (the apparent diameter of Jupiter was 39 arcsec) and the images are smeared with the Suzaku’s angular resolution of 120 arcsec.

Since Mars moved 27 arcmin per day during the observation, the spacecraft was repointed 27 times in 3 days to keep Mars within ~ 1.5 arcmin from the center of the XIS field-of-view (FOV) in order to avoid the vignetting effect, as summarized in table 1. Considering the small

¹ See §7.12 in the Suzaku technical description document
(http://www.astro.isas.ac.jp/suzaku/doc/suzaku_tsd/node10.html)

offset angle from the FOV center, the vignetting effect is almost negligible (See figure 11 in Serlemitsos et al. 2007). The XIS CCDs were operated in the normal mode. The net exposure time after the standard data screening was 82 ksec. We analyzed the screened data with the process of version 2.2.7.18 provided by the Suzaku processing facility, using the HEASoft version 6.4 package².

Figure 1 shows an XIS1 image in the 0.2–1 keV band. We adopted the XIS BI for the energy range of 0.2–1 keV and the FI for 1–5 keV, since the BI is more sensitive to < 1 keV while XIS FI is to > 1 keV. The first pointing was toward (RA, Dec)=(102°.886, 25°.171, J2000), (l , b)=(190°.245, 11°.205), while the last one was toward (RA, Dec)=(103°.964, 25°.48), (l , b)=(190°.776, 12°.040). No clear signals were detected at the expected positions of Mars (green circles) except for several point like sources in the hard energy band.

3. Image

In order to quantify the Martian X-ray emission in the X-ray images, we have to carefully exclude possible point sources in the trail of Mars and correct the data for the orbital motion of Mars. As a first step, we searched the image for bright sources (e.g. cluster of galaxies, supernova remnants and stars) using the bright X-ray source catalog compiled by NASA³. We found no point sources within the XIS FOVs in this catalog. Then, we identified possible faint point sources using the wavelet function program `wavdetect` in the CIAO package⁴. We created two images for 0.2–1 keV and 1–5 keV with different bin sizes (4.4 and 8.8 arcsec) to detect soft and hard X-ray sources and to take into account different point spread functions within the FOV. We ran the program by setting the significant threshold above 1×10^{-6} , which corresponds to one spurious source in each XIS FOV (1024×1024 pixels). We detected eleven point source candidates as shown in figure 1 (black circles). From the individual images in the 27 pointings, we confirmed that all these sources are bright in X-rays in relevant to the Martian orbit and the position of any point source candidate is fixed on the sky. Hence, we rejected a possibility that the point source candidates include short time variation(s) of the Martian X-ray emission. Their X-ray fluxes are $0.6 \sim 1 \times 10^{-13}$ erg cm⁻² s⁻¹ in 0.2–1.0 keV and $0.1 \sim 2 \times 10^{-13}$ erg cm⁻² s⁻¹ in 1–5 keV. Here we converted an XIS count rate into flux, assuming a power-law spectrum with a photon index of 1.4 and an average absorption column toward this field⁵, which represents a typical spectrum of the background active galactic nucleus. For comparison, we estimated the number of CXB (Cosmic X-ray Background) sources within the field of view (~ 0.37 deg²) based on Giacconi et al. 2001. The expected numbers became 9 and 90 if we assume the flux

² <http://heasarc.nasa.gov/lheasoft/>

³ http://heasarc.nasa.gov/cgi-bin/Tools/high_energy_source/high_energy_source.pl

⁴ <http://cxc.harvard.edu/ciao/index.html>

⁵ <http://heasarc.gsfc.nasa.gov/cgi-bin/Tools/w3nh/w3nh.pl>

limits of 1×10^{-13} and 1×10^{-14} erg cm $^{-2}$ s $^{-1}$ in 2–7 keV, respectively, while the observed numbers were 3 and 11. Thus, the source number seems inconsistent with the CXB estimation. This is more evident for faint sources, which may suggest that a part of the faint sources below 1×10^{-13} erg cm $^{-2}$ s $^{-1}$ in 2–7 keV are not point sources but fluctuations of the instrument background. Since we do not know which point sources are real, we decided to exclude all the X-ray sources in the following analysis, in order to avoid potential contamination. We excluded circular regions around individual sources with a diameter of 2 arcmin except for three bright sources, for which a 3 arcmin diameter region was utilized.

After removing the potential point sources, we checked each image and found that no significant X-ray emission is seen along the orbital path of Mars. To confirm this inspection, we corrected the images (figure 1) for the orbital motions of Mars and Suzaku in the same way as Ezoe et al. (2010). To take into account the excluded regions, we created exposure maps using `xisexpmapgen` and excluded the same regions from the exposure maps. Then, we transformed the exposure map considering Martian orbit and divided the orbital motion corrected image by the corrected map. The images corrected for the orbital motions are shown in figure 2. We chose two energy bands (0.2–1.0 keV and 0.5–0.65 keV), i.e., a broad charge exchange band and a narrower region, centered on the O VII line. However, no significant emission was seen at the position of Mars (green circle) in both energy bands.

4. Spectrum

To place a quantitative upper limit on the X-ray flux of Mars, we proceeded to a spectral analysis. In the same way as the imaging analysis (§3), we excluded the point source candidates from each event file for the 27 pointings without the correction for the orbital motions. We then extracted events from a circle region with a radius of 3 arcmin centered on Mars. This radius covers the orbital motion of Mars during each pointing (~ 3 arcmin) and considers the HPD. Background events were extracted from an annulus around Mars with a radius of 3 arcmin to 6 arcmin after subtracting the point sources.

Figure 3 shows the obtained X-ray spectra of Mars and the background. We can confirm that no significant emission is detected in 0.2–10 keV. A rise around 7–8 keV seen in both Mars and background spectra is most probably an instrumental Ni K $_{\alpha}$ line⁶. The 2σ upper limit of the Martian X-ray emission observed near Earth in the O VII band (0.5–0.65 keV) was 1.7×10^{-3} [cts s $^{-1}$], corresponding to the photon flux of 4.3×10^{-5} [photon cm $^{-2}$ s $^{-1}$]. The upper limits in three energy bands are summarized in table 2.

⁶ http://heasarc.nasa.gov/docs/astroe/prop_tools/suzaku_td/node10.html

5. Discussion

Below we would like to discuss Martian X-ray emission in the context of the scattering of solar X-rays and the exospheric solar wind charge exchange. In order to comprehensively understand the characteristics of Martian X-ray emission, we compared our result with the past Chandra observation at solar maximum (Dennerl 2002) and the XMM-Newton observation at the intermediate state (Dennerl et al. 2006). We also utilized the solar wind data taken with the ACE satellite and the solar X-ray flux measured with GOES-12.

5.1. Scattering of solar X-rays

We firstly estimated the fluorescent X-ray flux due to the scattering of solar X-rays by the upper Martian atmosphere. This component depends on the amount of the incident solar X-rays during the observation. Figure 4 shows the GOES-12 solar X-ray flux in 2001-2008. The Suzaku observation corresponds to the solar minimum phase when the solar X-ray flux is significantly lower than those in the other two Chandra and XMM-Newton observations. Close-up views during the three observations are shown in figure 5. We averaged the solar X-ray fluxes during the observation time. The average solar X-ray fluxes were $3.1 \times 10^{-7} \text{ W m}^{-2}$ (Chandra), $2.5 \times 10^{-6} \text{ W m}^{-2}$ (XMM-Newton) and $3.1 \times 10^{-8} \text{ W m}^{-2}$ (Suzaku). Thus, the solar X-ray at the Suzaku observation is 10 times lower than the Chandra and 100 times lower than the XMM-Newton.

The observed fluorescent X-ray flux from Mars in O VII band (0.5–0.65 keV) derived from the section 3.2 of Dennerl (2002) and the column (c) in table 2 of Dennerl et al. (2006) with the Suzaku response was 5.5×10^{-5} and $3.7 \times 10^{-5} \text{ cts cm}^{-2} \text{ s}^{-1}$ in the Chandra and XMM-Newton observations, respectively. By taking into account the solar X-ray flux, the phase angle, and the distance of Earth-Mars and Sun-Mars, the fluorescent X-ray flux during the Suzaku observation is estimated. The positions of the X-ray observatories, Sun and Mars in the three observations are shown in figure 6. The phase angle was 18.2, 41.2 and 37.0 degree in the Chandra, XMM-Newton, and Suzaku observations, respectively, while the geocentric distance of Mars was 0.5, 0.8 and 1.4 AU, and the heliocentric distance was 1.4, 1.4, and 1.7 AU. Provided that the phase angle is the same as that in the Suzaku observation from figure 12 in Dennerl (2002), the photon fluxes of the Chandra and XMM-Newton observations, are converted into 4.9×10^{-5} and $3.8 \times 10^{-5} \text{ cts cm}^{-2} \text{ s}^{-1}$, respectively. In addition, by considering the solar X-ray flux, and the geocentric and heliocentric distances, the expected photon fluxes become 4.2×10^{-7} and $1.1 \times 10^{-7} \text{ cts cm}^{-2} \text{ s}^{-1}$, respectively. These values are more than an order of magnitude lower than the 2σ upper limit of $4.3 \times 10^{-5} \text{ ph cm}^{-2} \text{ s}^{-1}$. Therefore, the scattering of solar X-rays during the Suzaku observation should be small.

5.2. Solar wind charge exchange

We next estimate the charge exchange emission. Here, we simply assume that only a single charge exchange occurs while the highly charged ions in the solar wind go through the Martian atmosphere, from the analogy with the charge exchange emission of moderately active comets and the Earth's exosphere (Cravens 1997; Cravens et al. 2001). We can express the X-ray volume emissivity $P_x = \alpha n_{\text{sw}} u_{\text{sw}} n_{\text{n}}$ [eV cm⁻³ s⁻¹], where n_{sw} , u_{sw} , and n_{n} are the solar wind proton density, solar wind speed, and neutral target density that is in the collisionally thin regions of the Martian exosphere, respectively. The parameter α is given as $\alpha \approx f_{\text{h}} < \sigma_{\text{cx}} > E_{\text{ave}}$, where f_{h} is a fraction of heavy ions in the solar wind, $< \sigma_{\text{cx}} >$ is an average cross section of charge exchange for all species and charge state, and E_{ave} is an average photon energy. By integrating this equation in the line of sight and dividing it by the solid angle, we can obtain the X-ray energy flux. Hence, we assume that the X-ray flux is proportional to the incident solar wind flux and the exospheric density integrated in the line of sight. According to a Chamberlain exospheric model (Chamberlain & Hunten 1987), the exospheric density will depend on the density and temperature at the exobase. Here we assume the fixed scale height for simplicity. Thus, when the density is increased by inserting additional particles into the atmosphere, the charge exchange X-ray flux would also increase. Therefore, the X-ray observations can provide a means of remotely estimating the condition of the exosphere.

Below we place an upper limit on the exospheric density by comparing the Suzaku observation with the past Chandra and XMM-Newton observations. We used the solar wind proton flux obtained with ACE SWEPAM⁷ to estimate the incident solar wind heavy ions. Although the proton flux, which is a proxy for the heavy ions in the solar wind, is not very strongly correlated with the heavy ion flux (Neugebauer et al. 2000), the sparse and not always available ACE SWICS O⁺⁷ data during the X-ray observations hindered us to directly estimate the heavy ion flux. In addition to these data, we used the in situ solar wind proton flux using the ASPERA-3 instrument onboard Mars Express (Barabash et al. 2006). While the data on April 3 was lost because of the overwrite in the onboard data recorder, we get the solar wind flux on April 4 and 5 (blue symbols in figure 7c). The fluxes are consistent with the estimated fluxes using ACE. Note that Mars Express was not in orbit during the Chandra and XMM-Newton observations. We considered arrival times of the solar wind depending on the locations of Earth, Mars and the ACE satellite that orbits around a Lagrangian point (L1) between the Sun and Earth (1.5 million km away from Earth), when we estimate the average proton flux. When Mars is in the upstream side of the solar wind compared to Earth, the solar wind which hits Mars will arrive Earth at $t_{\text{E}} = t_{\text{M}} + \Delta t$, where t_{E} , t_{M} and Δt are the arrival times at Earth and Mars, and the expected time delay, respectively. The expected time delay can be expressed as $\Delta t = \theta/\Omega - (\Delta r_{\text{EM}} + \Delta r_{\text{EA}})/u_{\text{sw}}$ based on Neugebauer et al. 2000, where θ is

⁷ <http://www.srl.caltech.edu/ACE/ASC/level2/index.html>

the difference in the heliographic longitudes of Earth and Mars, $\Omega = 14.7^\circ/\text{day}$ is the rotational speed of the Sun, Δr_{EM} is the difference of the heliocentric distances of Earth and Mars, and $\Delta r_{\text{EA}} = 1.5 \times 10^6$ [km] is the distance between Earth and the ACE satellite. We thus estimated the proton density and speed at the time of the Mars observations considering the time delay. Moreover, we corrected the proton density for the difference of the heliocentric distances of Mars and the ACE satellite. Figure 7 shows the solar wind proton flux at t_{M} in the Chandra, XMM-Newton and the Suzaku observations. Table 3 summarizes the average proton flux at t_{M} , distances, and the observed X-ray fluxes with the three observatories.

We then compared the 0.5–0.65 keV X-ray flux during the Suzaku observation with those in the Chandra and XMM-Newton observations. The 0.5–0.65 keV X-ray fluxes in the Chandra and XMM-Newton observations were estimated from the halo model in section 3.2 of Dennerl (2002) and in the column (c) in table 2 of Dennerl et al. (2006), respectively. Simply from the geocentric distances, the expected X-ray flux during the Suzaku observation becomes 0.1 and 0.3 times smaller than those of Chandra and XMM-Newton, respectively. The proton flux corresponding to the Suzaku observation was 0.8 and 0.5 times those of Chandra and XMM-Newton. Then, the expected X-ray flux during the Suzaku observation is still 0.1 and 0.2 times smaller than those of Chandra and XMM-Newton, respectively. Therefore, if we assume that the solar wind heavy ion flux scaled with the proton flux and that the ionization states were similar during the three observations, the undetection of the Martian halo emission with Suzaku means that the exospheric density at solar minimum is not significantly higher than those at solar maximum. We estimate an upper limit of the exospheric neutral density during the Suzaku observation as 70 and 6 times during the Chandra and XMM-Newton observations. This result places a 2σ limit on the modeling of the Martian exosphere and can not reject the higher exospheric density at lower solar activity.

6. Summary

We investigated the Martian X-ray emission with Suzaku XIS in 2008 April. For the first time, we observed Mars at solar minimum. We carefully excluded possible point sources from the XIS 0.2–1 and 1–5 keV images and corrected the data for the point sources and the orbital motion of Mars. We analyzed the X-ray image and spectrum, and concluded that there was no significant X-ray flux from Mars observed by Suzaku. We placed stringent upper limits on the Martian X-ray flux around the O VII band (0.5–0.65 keV). We compared the upper limit with the past Chandra and XMM-Newton detections of the Martian X-ray emission consisting of the scattering of solar X-rays by the planet’s body and the solar wind charge exchange halo. Using the simultaneously obtained solar X-ray and wind data, we estimated that the fluorescent emission due to the scattering must be negligible, and placed an upper limit on the Martian exospheric density from the X-ray data as 70 and 6 times during the Chandra and XMM-Newton observations, respectively.

Acknowledgments. We thank the ACE SWEPAM instrument team and Dr. K. Dennerl for valuable comments. This work was supported by Grant-in-Aid for JSPS Fellows.

References

- Anderson, D. E. 1974, *J. Geophys. Res.*, 79, 1513.
- Barabash, S., et al. 2006, *Space Science Reviews*, 126, 113.
- Chamberlain, J.W., Hunten, D.M. 1987, *Theory of Planetary Atmospheres*, (San Diego, CA: second ed Academic Press), 335
- Chaufray, J.Y., Bertaux, J.L., Leblanc, F., Quémerais, E. 2008, *Icarus*, 195, 598.
- Cravens, T.E. 1997, *J. Geophys. Res. Lett.*, 24, 105.
- Cravens, T.E., Robertson, I.P., & Snowden, S.L., 2001, *J. Geophys. Res.* 106, 24883.
- Dennerl, K., Englhauser, J., & Trümper, J. 1997, *Science*, 277, 1625.
- Dennerl, K. 2002, *A&A*, 394, 1119.
- Dennerl, K., Burwitz, V., Englhauser, J., Lisse, C., & Wolk, S. 2002, *A&A*, 386, 319.
- Dennerl, K., et al. 2006, *A&A*, 451, 709.
- Ezoe, Y., Ishikawa, K., Ohashi, T., Miyoshi, Y., Terada, N., Uchiyama, & Y., Negoro, H. 2010, *ApJ*, 709, L178.
- Galli, A., et al. 2006, *Space Science Reviews*, 126, 447.
- Giacconi, R., et al. 2001, *ApJ*, 551, 624.
- Gladstone, G.R., et al. 2002, *Nature*, 415, 1000.
- Grader, R.J., Hill, R.W., & Seward, F.D. 1968, *J. Geophys. Res.* 73, 7149.
- Holmström, M., & Barabash, S. 2001, *Geophys. Res. Lett.*, 28, 1287.
- Koyama, K., et al. 2007, *PASJ*, 59, S23.
- Krasnopolsky, V.A., & Gladstone, G.R. 1996, *J. Geophys. Res.*, 101, 765.
- Krasnopolsky, V.A. 2002, *J. Geophys. Res.*, 107, 5128.
- Krasnopolsky, V.A., Greenwood, J.B., & Stancil, P.C. 2004, *Space Sci. Rev.*, 113, 271.
- Mitsuda, K., et al. 2007, *PASJ*, 59, S1.
- Ness, J.-U., Schmitt, J.H.M.M., & Robrade, J. 2004, *A&A*, 414, L49.
- Neugebauer, T., Cravens, T.E., Lisse, C.M., Ipavich, F.M., Christian, D., von Steiger, R., Bochsler, P., Shah, P.D., & Armstrong, T.P. 2000, *J. Geophys. Res.*, 105, 20,949.
- Serlemitsos, P.J., et al. 2007, *PASJ*, 59, S9.
- Uchiyama, Y., et al. 2008, *PASJ*, 60, S35.
- Wegmann, R., Schmidt, H.U. , Lisse, C M., Dennerl, K., & Englhauser, J. 1998, *Planet. Space. Sci.*, 46, 603

Table 1. Summary of the time of the individual pointings.

Pointing ID	Begin [UT]	End [UT]	Exposure time [s]
1	April 3 08:11:44	April 3 09:50:19	2913
2	April 3 09:50:32	April 3 11:50:19	4887
3	April 3 11:50:28	April 3 13:50:19	3910
4	April 3 13:50:32	April 3 15:50:19	2288
5	April 3 15:50:28	April 3 17:50:16	1368
6	April 3 17:50:33	April 3 19:50:18	1939
7	April 3 19:50:31	April 3 21:40:18	2511
8	April 3 21:40:31	April 4 00:10:24	5608
9	April 4 00:10:37	April 4 01:50:24	2175
10	April 4 01:50:33	April 4 03:50:24	3772
11	April 4 03:50:33	April 4 05:50:24	4620
12	April 4 05:50:37	April 4 07:50:24	3455
13	April 4 07:50:33	April 4 09:50:24	4252
14	April 4 09:50:37	April 4 11:50:24	4825
15	April 4 11:50:33	April 4 13:50:24	3831
16	April 4 13:50:37	April 4 15:50:24	1440
17	April 4 15:50:33	April 4 17:50:20	1978
18	April 4 17:50:37	April 4 19:50:04	1862
19	April 4 19:50:21	April 4 21:50:14	1700
20	April 4 21:50:27	April 4 23:50:14	1849
21	April 4 23:50:23	April 5 01:50:14	2881
22	April 5 01:50:27	April 5 03:50:14	4025
23	April 5 03:50:27	April 5 05:50:14	4519
24	April 5 05:50:27	April 5 07:50:14	3423
25	April 5 07:50:23	April 5 09:50:14	4261
26	April 5 09:50:27	April 5 11:50:14	4798
27	April 5 11:50:23	April 5 13:00:13	1100

Table 2. 2σ upper limits of the Martian X-ray emission^a.

energy band [keV]	count rate [cts s ⁻¹]	photon flux [photon cm ⁻² s ⁻¹]
0.5–0.65	1.7×10^{-3}	4.3×10^{-5}
0.2–1.0	4.3×10^{-3}	2.3×10^{-4}
1.0–5.0	6.7×10^{-3}	3.5×10^{-5}

^a The BI data was used for 0.5–0.65 and 0.2–1.0 keV, while the FI was used for 1.0–5.0 keV.

Table 3. Summary of solar activity for Chandra, XMM-Newton and Suzaku. X-ray flux is in 0.5-0.65 keV.

	observation date	proton flux ^a (cm ⁻² s ⁻¹)	Earth-Mars/Sun-Mars (AU)	X-ray flux (photon cm ⁻² s ⁻¹)
Chandra	2001/07/04	1.3×10 ⁸	0.5/1.4	5.8×10 ⁻⁶
XMM-Newton	2003/11/19-21	2.2×10 ⁸	0.8/1.4	3.8×10 ⁻⁵
Suzaku	2008/04/03-05	1.0×10 ⁸	1.4/1.7	<4.3×10 ⁻⁵

^a The proton flux is estimated by considering the arrival time and the heliospheric distance (see text).

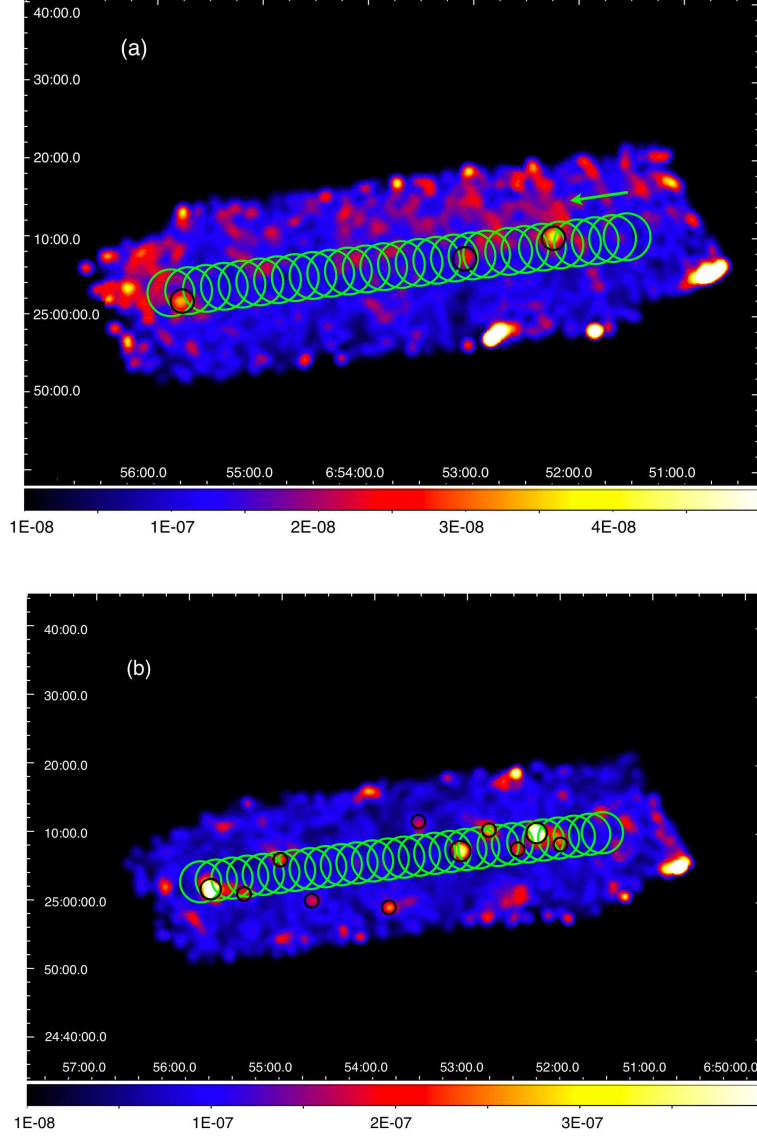


Fig. 1. An XIS mosaic image in 0.2–1 keV (panel a, BI) and 1–5 keV (panel b, FI) displayed on the J2000.0 coordinate. Images are corrected by exposure time and a count unit is counts s^{-1} binned pixel^{-1} . For clarity, the image is binned by a factor of 8 (8 arcsec) and smoothed by a Gaussian of $\sigma = 5$ pixels (5.3 arcsec). An arrow indicates the moving direction of Mars. A green circle displays the positions of Mars. Its radius is 3 arcmin, corresponding the sum of HPD (Half Power Diameter; 2 arcmin) of Suzaku and the moving step for the attitude shift. Black circles represent possible point sources that are excluded for further analysis.

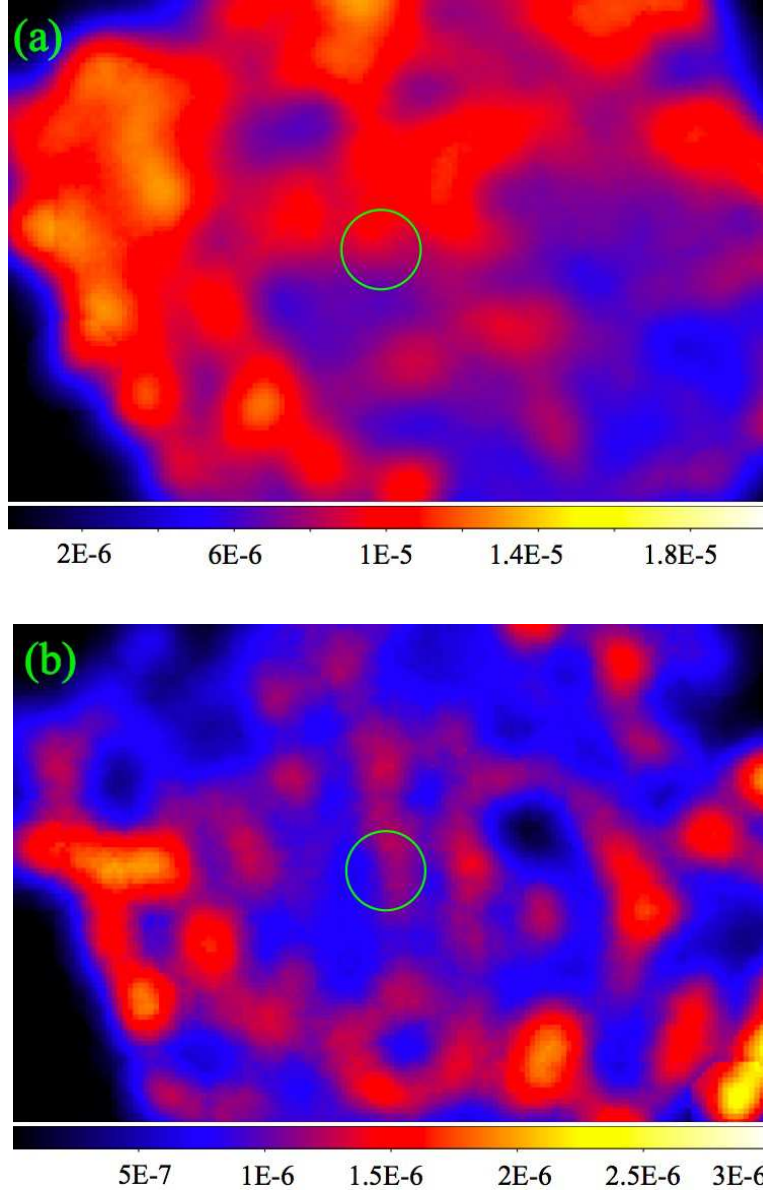


Fig. 2. XIS images after correction for the orbital motion of Suzaku and Mars's ephemeris (<http://ssd.jpl.nasa.gov/horizons.cgi>) in 0.2–1 keV (panel a) and in 0.5–0.65 keV (panel b). Images are binned and smoothed in the same way as figure 1. Green circles indicate the expected position of Mars. Its diameter is 2 arcmin considering the HPD and pointing uncertainty of Suzaku (~ 20 arcsec in radius) (Uchiyama et al. 2008).

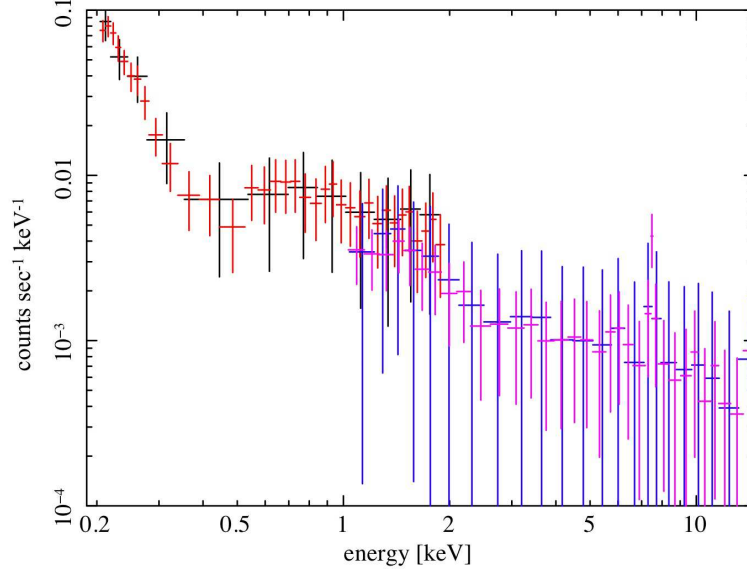


Fig. 3. XIS spectra of Mars compared to the surrounding background. The BI CCD spectra are shown in black (Mars) and red (background), while the FI spectra are shown in blue (Mars) and magenta (background). An error is 1σ significance.

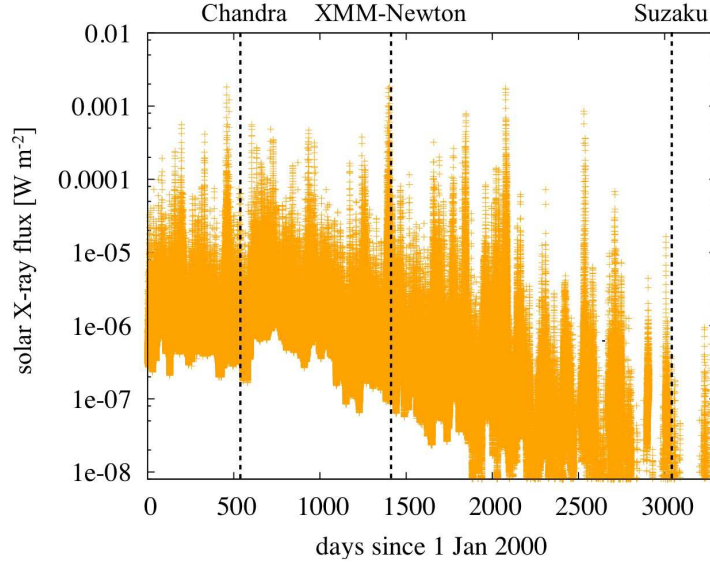


Fig. 4. The solar X-ray flux from 2000 January 1 to 2008 December 31 measured with GOES-12 1.0-8.0Å.

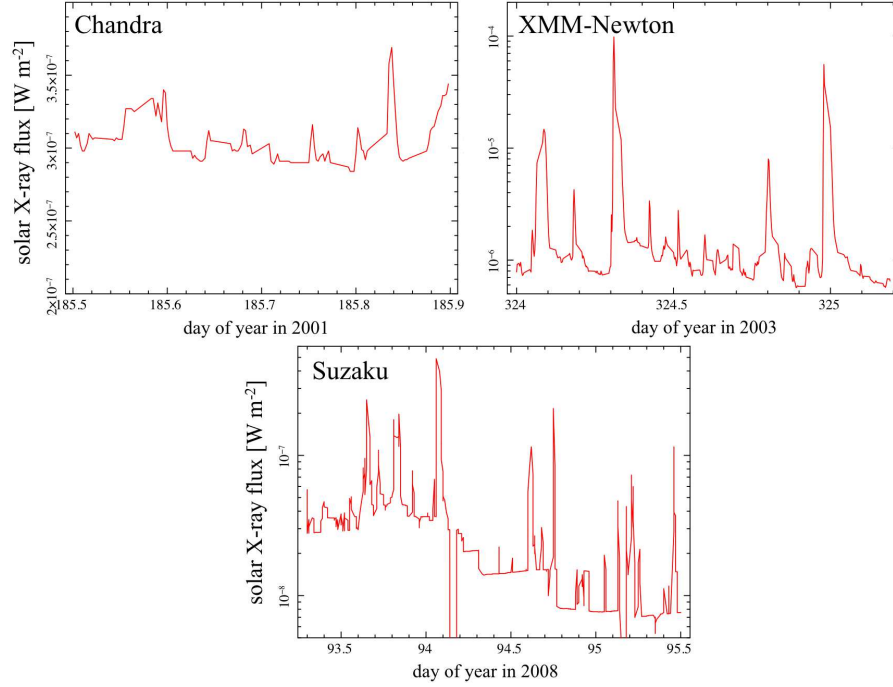


Fig. 5. The same as figure 4 but close-up views for the Chandra (top left), XMM-Newton (top right), and Suzaku (bottom) observations. The vertical scale is linear for the Chandra panel but logarithmic for the others.

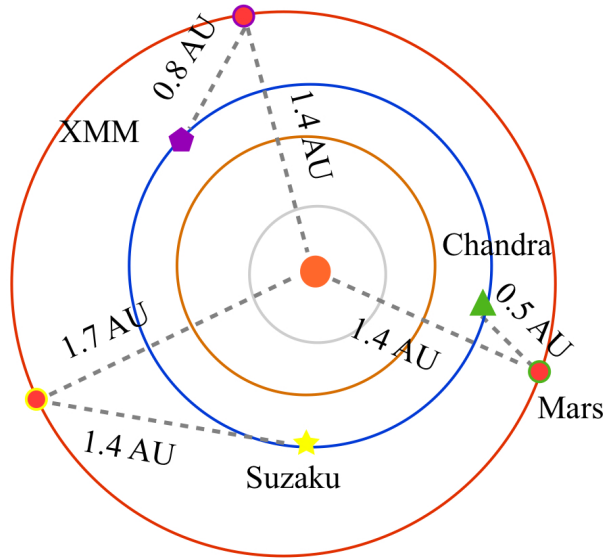


Fig. 6. Positions of Sun, Mars and X-ray observatories in the three observations (<http://space.jpl.nasa.gov/>). An orange circle indicates Sun, while red circles represent Mars. A blue circle shows an orbit of Earth, and symbols along the blue circle shows positions of the three observatories. A pentagon is XMM-Newton, a triangle is Chandra and a star is Suzaku.

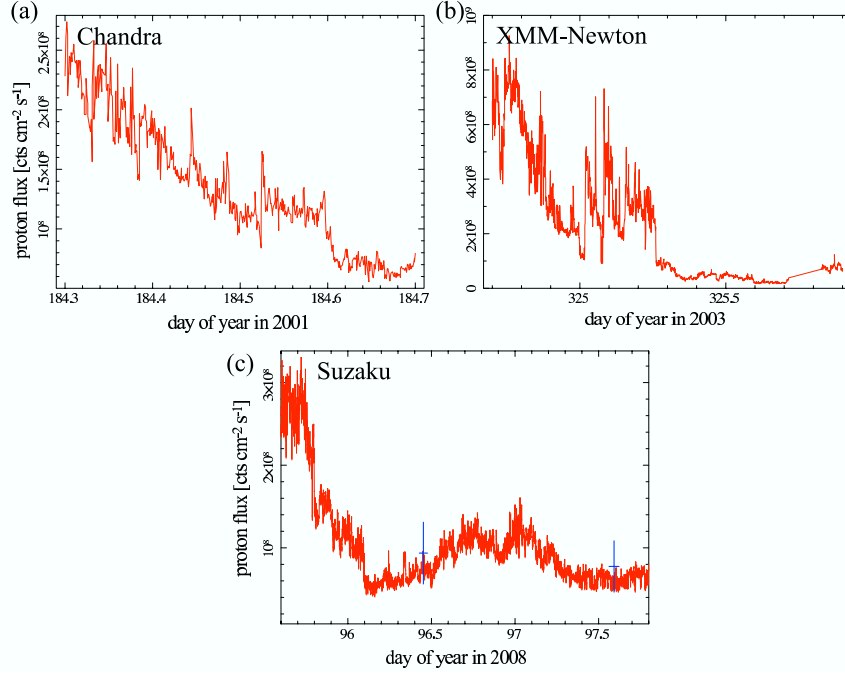


Fig. 7. The solar wind proton flux measured by the ACE satellite corresponding to the Chandra (panel a), XMM-Newton (panel b), and Suzaku (panel c) observations. The observed data is shifted in time considering the propagation time of the solar wind to Mars. In situ solar wind flux observed by ASPERA-3 is shown by blue symbols.